

## Article

# Photocatalytic Degradation of Tartrazine and Naphthol Blue Black Binary Mixture with the TiO<sub>2</sub> Nanosphere under Visible Light: Box-Behnken Experimental Design Optimization and Salt Effect

Fadimatou Hassan <sup>1,2</sup>, Bouba Talami <sup>1,2</sup>, Amira Almansba <sup>3</sup>, Pierre Bonnet <sup>4,\*</sup>, Christophe Caperaa <sup>4</sup> ,  
Sadou Dalhatou <sup>2,\*</sup> , Abdoulaye Kane <sup>1</sup>  and Hicham Zeghioud <sup>1,\*</sup> 

<sup>1</sup> UniLaSalle-Ecole des Métiers de l'Environnement, Cyclann, Campus de Ker Lann, 35170 Bruz, France; abdoulaye.kane@unilasalle.fr (A.K.)

<sup>2</sup> Department of Chemistry, Faculty of Science, University of Maroua, Maroua 814, Cameroon

<sup>3</sup> Laboratory of Industrial Process Engineering Sciences, University of Sciences and Technology Houari Boumediene, Algiers 16111, Algeria

<sup>4</sup> Institut de Chimie de Clermont-Ferrand, Université Clermont Auvergne, 63000 Clermont-Ferrand, France

\* Correspondence: pierre.m.bonnet@uca.fr (P.B.); sadou.dalhatou@fs.univ-maroua.cm (S.D.); hicham.zeghioud@unilasalle.fr or hicheming@yahoo.fr (H.Z.)



**Citation:** Hassan, F.; Talami, B.; Almansba, A.; Bonnet, P.; Caperaa, C.; Dalhatou, S.; Kane, A.; Zeghioud, H. Photocatalytic Degradation of Tartrazine and Naphthol Blue Black Binary Mixture with the TiO<sub>2</sub> Nanosphere under Visible Light: Box-Behnken Experimental Design Optimization and Salt Effect. *ChemEngineering* **2024**, *8*, 50. <https://doi.org/10.3390/chemengineering8030050>

Academic Editors: Chrysoula Athanasekou, Alirio E. Rodrigues and Nikolaos G. Moustakas

Received: 29 January 2024

Revised: 12 April 2024

Accepted: 25 April 2024

Published: 3 May 2024



**Copyright:** © 2024 by the authors. Licensee MDPI, Basel, Switzerland. This article is an open access article distributed under the terms and conditions of the Creative Commons Attribution (CC BY) license (<https://creativecommons.org/licenses/by/4.0/>).

**Abstract:** In this study, TiO<sub>2</sub> nanospheres (TiO<sub>2</sub>-NS) were synthesized by the solvothermal method. Firstly, the synthesized nanomaterial was characterized by X-ray diffraction (XRD), Fourier Transformed Infrared (FTIR), scanning electron microscopy (SEM) and UV-Vis Diffuse Reflectance Spectroscopy (DRS). To study the photocatalytic degradation of Tartrazine (TTZ) and Naphthol Blue Black (NBB) in a binary mixture, the influence of some key parameters such as pH, pollutant concentration and catalyst dose was taken into account under visible and UV light. The results show a 100% degradation efficiency for TTZ after 150 min of UV irradiation and 57% under visible irradiation at 180 min. The kinetic study showed a good pseudo-first-order fit to the Langmuir–Hinshelwood model. Furthermore, in order to get closer to the real conditions of textile wastewater, the influence of the presence of salt on TiO<sub>2</sub>-NS's photocatalytic performance was explored by employing NaCl as an inorganic ion. The optimum conditions provided by the Response Surface Methodology (RSM) were low concentrations of TTZ (2 ppm) and NBB (2.33 ppm) and negligible salt (NaCl) interference. The percentage of photodegradation was high at low pollutant and NaCl concentrations. However, this yield became very low as NaCl concentrations increased. The photocatalytic treatment leads to 31% and 53% of mineralization yield after 1 and 3 h of visible light irradiation. The synthesis of TiO<sub>2</sub>-NS provides new insights that will help to develop an efficient photocatalysts for the remediation of contaminated water.

**Keywords:** TiO<sub>2</sub> nanospheres; photodegradation; response surface methodology; dyes

## 1. Introduction

World population growth and climate change have given rise to an alarming decline in freshwater resources and their availability [1], thus posing a major challenge worldwide. The increase in industrialization, urbanization, and unlimited anthropogenic activities has led to the generation of wastewater originating from various manufacturing [2] and processing industries, such as petroleum hydrocarbons [3], textile, agriculture, dyeing, cosmetics, food, and pharmaceuticals [4].

The contamination of water by emerging pollutants is a major environmental concern. Emerging pollutants refer to contaminants for which there is currently no regulation requiring monitoring, or public reporting of their presence in our water supply or wastewaters. There are many types, such as pesticides, pharmaceuticals, drugs, cosmetics, personal

care products, surfactants, cleaning products, industrial formulations and chemicals, food additives, food packaging, metalloids, rare earth elements, nanomaterials, microplastics, pathogens, and dyes [5–7]. Their main sources are domestic discharges, hospital effluents, landfill leachates, livestock and aquaculture, and agricultural and industrial wastewaters [5]. Therefore, dyes released into the environment via wastewater cause a major problem in water quality and, consequently, human health. For instance, TTZ [8] and NBB [9,10], the model compounds for this study, are acid azo dyes with sulfonic groups acting as auxochromes that are highly water-soluble and have high stability. Unfortunately, their by-products are known to be mutagenic and carcinogenic aromatic compounds [11].

The removal of these toxic organic pollutants from water is essential to ensuring sustainable water remediation and management [12]. On this basis, water treatment methods such as advanced oxidation processes (AOPs) have been used so far, and are considered to be the best method for treating organic wastewater. This is due to their high mineralization efficiency [13], rapid oxidation reaction rate, and potential for use in treating a wide range of emerging contaminants not treatable by conventional techniques [14]. They are implicated in the oxidation via mineralization of organic pollutants by generating reactive oxygen species (ROS), including hydroxyl radicals ( $\text{HO}^\bullet$ ) and sulfates [15]. Photocatalysis among AOPs has proven to be a potential means for the elimination of micropollutants present in water [16]. The photocatalysis process is based on the photoexcitation of a semiconductor by light irradiation (ultraviolet light (UV) or visible light (VL)) to degrade organic pollutants into  $\text{CO}_2$  and  $\text{H}_2\text{O}$  [17].

The use of semiconductors such as  $\text{TiO}_2$ ,  $\text{ZnO}$ ,  $\text{Fe}_2\text{O}_3$ ,  $\text{ZnS}$ , and  $\text{V}_2\text{O}_5$  has been reported in the literature for their use in wastewater treatment [18–22]. Titanium dioxide ( $\text{TiO}_2$ ) is one of the most studied metal oxide photocatalysts, thanks to its high chemical stability and excellent photocatalytic activity. Photodegradation using  $\text{TiO}_2$  as a catalyst has attracted extensive interest owing to its great advantages (optical–electronic properties, low-cost, chemical stability, and non-toxicity) related to the complete removal of organic pollutants from wastewater. Interest also comes from its efficiency and high availability compared to other semiconductors. The high photocatalytic activity of  $\text{TiO}_2$  has been strongly recognized in the literature [23–25].

Owing to its large band gap (3.0–3.2 eV) [26],  $\text{TiO}_2$  has some limitations, such as rapid electron hole recombination and low quantum yield, and it can only be excited by UV light irradiation, which is only about 5% of the solar power spectrum [27]. To address this problem, efforts have been made to modify  $\text{TiO}_2$  to increase visible light absorption by modifying its nanostructures. Various methods of producing  $\text{TiO}_2$  nanoparticles with improved and large surface areas exist, such as solvothermal methods, the sol-gel method, chemical precipitation, and ultrasonic irradiation [28,29]. The most common methods used to improve the photocatalytic efficiency of  $\text{TiO}_2$  involve increasing its photoresponse range and reducing photogenerated-carrier coupling. The morphology, size, and structure of a heterojunction can be modified by doping with elements, thereby improving photocatalytic efficiency. These methods have made it possible to synthesize various  $\text{TiO}_2$ -based nanoparticles and apply them in photocatalysis, in particular  $\text{TiO}_2$  nanorods [30],  $\text{TiO}_2$  nanosheets [31],  $\text{TiO}_2$  nanofibers [32],  $\text{TiO}_2$  nanowires [33],  $\text{TiO}_2$  nanotubes [34], and  $\text{TiO}_2$  nanospheres [35]. Studies report that the use of spherical mesoporous  $\text{TiO}_2$  nanostructures enhances mass and charge transfers within the porous regions during photocatalytic reactions [36]. Moreover, it has been observed that catalysts with spherical shapes larger than 200 nm facilitates easy separation and reusability [37].

In this work, the solvothermal method has been used to synthesize  $\text{TiO}_2$ -NS, as a simple method for the preparation of visible light-active photocatalysts.  $\text{TiO}_2$ -NS was characterized by different techniques, and its photocatalytic performance was examined in relation to the degradation of a binary dye solution of Tartrazine and Naphthol Blue Black as target pollutants. Response surface methodology (RSM) was used as an efficient tool to study the effects of key parameters and highlight the optimum conditions. Finally,

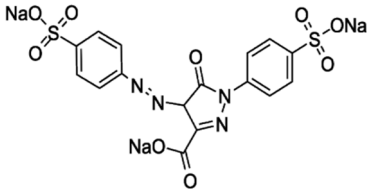
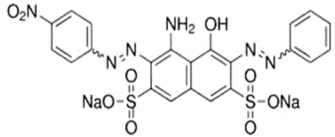
the mineralization performances of photocatalysts in TTZ elimination, in addition to stability and reusability, were addressed.

## 2. Material and Method

### 2.1. Reagents

Naphthol Blue Black, Titanium (IV) isopropoxide 97% and Sodium chloride (NaCl  $\geq$  99.0%) were purchased from SIGMA-ALDRICH Corporation (Saint-Louis, MO, USA) Tartrazine dye powder were purchased from ThermoScientific Chemicals (Haverhill, MA, USA), hydrochloric acid (HCl  $\geq$  37%) was purchased from Honeywell (Diegem, Belgium), hydroxide sodium (NaOH  $\geq$  98%) was from Organics (Chicago, IL, USA) and Isopropanol (CH<sub>3</sub>CH(OH)CH<sub>3</sub>  $\geq$  99.7%) was obtained from MERCK Company (Darmstadt, Germany). These were all used for this study. The physico-chemical properties of Tartrazine and Naphthol Blue Black are listed in Table 1.

**Table 1.** Physico-chemical properties of dyes.

Dye	Molecular Formula	Structure	$\lambda_{\max}$ (nm)
Tartrazine	C <sub>16</sub> H <sub>9</sub> N <sub>4</sub> Na <sub>3</sub> O <sub>9</sub> S <sub>2</sub>		426
Naphthol Blue Black	C <sub>22</sub> H <sub>14</sub> N <sub>6</sub> Na <sub>2</sub> O <sub>9</sub> S <sub>2</sub>		618

### 2.2. Catalyst Synthesis

TiO<sub>2</sub>-NS was prepared according to the protocols found in the literature [38]. Into 35 mL of ethanol, 10 mL of Titanium (IV) isopropoxide was added dropwise under stirring, which resulted in a white suspension. Ultrapure water (5 mL) was also added dropwise into the suspension and stirred continuously for 2 h. The suspension was heated at 115 °C for 12 h in a Teflon-lined autoclave reactor, then filtered and washed several times with ultrapure water. The TiO<sub>2</sub> nanospheres obtained were dried at 100 °C for 12 h and then calcined at 350 °C for 3 h in air.

### 2.3. Characterization

The specific surface area was studied by the Brunauer–Emmett–Teller (BET) method with the ASAP 2020 V4.04 (V4.04 H) apparatus. The structural changes in TiO<sub>2</sub> nanospheres were examined using a Jobin Yvon Raman spectrophotometer model T64000. The laser wavelength was 514.5 nm (2.41 eV), and the power was 100 mW. The measurement was carried out in the solid state by dispersing the sample powder on a glass solid in air at room temperature. Fourier transform infrared (FT-IR) analysis was utilized to evaluate the surface chemistry or the functional groups of the synthesized materials. This analysis was carried out with an average of 128 scans in ATR mode with a diamond crystal from 4000 to 400 cm<sup>-1</sup>. The synthesized TiO<sub>2</sub>-NS was structurally and morphologically characterized by scanning electron microscopy (SEM) using a JEOL 6060-LV apparatus. The UV-Vis diffuse reflectance spectra (UV-Vis DRS) of the synthesized material were recorded with a Cary 300 instrument with a scan rate of 600 nm/min. The fluorescence X was used to determine the chemical composition of the samples using a Panalytical Epsilon 3 with an Ag anode tube. Pollutant concentration was monitored using a UV-Vis spectrophotometer

SHIMADZU UV-1800 (Marne La Vallée, France) and mineralization was assessed using a VCSn TOCmeter SHIMADZU (Marne La Vallée, France).

#### 2.4. Photocatalytic Treatment

The photocatalytic degradation efficiency of TiO<sub>2</sub>-NS was assessed via the photodegradation of Tartrazine (TTZ) and a binary mixture of Tartrazine (TTZ) and Naphthol Blue Black (NBB) dye solution. Visible light ( $\lambda_{\text{max}} = 800 \text{ nm}$ ) and ultraviolet light ( $\lambda_{\text{max}} = 254 \text{ nm}$  of UV-C), from sources with 11 W of power, were used in performing the Tartrazine photodegradation, and a visible light source was used for the photodegradation of the binary mixture. A TTZ solution (5 ppm) was prepared, and binary mixture solutions used in the experiments were also prepared at different concentrations (with a molar concentration of 1:1 ratio). A mass of the catalyst was dispersed into 200 mL of solutions. The mixture was left in the dark and continuously stirred at 900 rpm for 60 min to achieve adsorption–desorption equilibrium before light irradiation. After reaching the adsorption–desorption equilibrium, the dye solution was exposed to light for 180 min. At 30 min time intervals, 3 mL samples of the solution were collected from the photoreactor and filtered to remove the photocatalysts using a syringe filter (pore size 0.45  $\mu\text{m}$ ). A spectrophotometer (SHIMADZU UV-1800) was used to measure the absorbances of TTZ and NBB at their maximum absorption peak intensity ( $\lambda_{\text{max}}$ ) values of 426 nm and 618 nm, respectively. The photocatalytic degradation and the mineralization were estimated using Equations (1a) and (1b), respectively.

$$R(\%) = \frac{C_0 - C_t}{C_0} \times 100 \quad (1a)$$

$$\text{Mineralization}(\%) = \frac{\text{TOC}_0 - \text{TOC}_t}{\text{TOC}_0} \times 100 \quad (1b)$$

where  $C_0$  and  $C_t$  are the initial concentration and concentration at time  $t$ , in mg/L of pollutant, respectively. The  $\text{TOC}_0$  and  $\text{TOC}_t$  are the total organic carbon values at time 0 min and  $t$ , respectively.

### 3. Results and Discussions

#### 3.1. Characterization

##### 3.1.1. X-ray Diffraction, Raman Spectroscopy, Fourier Transformer Infrared (FTIR) and X-ray Fluorescence of TiO<sub>2</sub>-NS

The XRD diffractograms of TiO<sub>2</sub> nanospheres are shown in Figure 1a. Peaks at  $2\theta$  equal to  $25.2^\circ$ ,  $37.9^\circ$ ,  $48.1^\circ$ ,  $53.9^\circ$ ,  $55.1^\circ$ ,  $62.8^\circ$ , and  $68.9^\circ$ , corresponding to the (101), (112), (200), (105), (211), (204), and (116) planes, respectively, are attributed to the anatase phase of TiO<sub>2</sub> [39,40]. Figure 1b shows the Raman spectra of the prepared TiO<sub>2</sub> nanospheres. The bands observed around 394, 513, and 637  $\text{cm}^{-1}$  correspond to the anatase crystalline phase of TiO<sub>2</sub>, which are related to the B<sub>1g</sub>, A<sub>1g</sub>, and E<sub>g</sub> Raman modes, respectively [41]. No peaks characteristic of other phases or impurities were detected, indicating that the prepared TiO<sub>2</sub> nanospheres obtained were of high purity. The broadening of the Raman spectroscopy peaks can be attributed to the size of the TiO<sub>2</sub> nanocrystals. Figure 1c shows the FTIR peaks of TiO<sub>2</sub> nanospheres. We only observe bands around 421  $\text{cm}^{-1}$ , which can be attributed to Ti–O stretching vibrations [42]. These results are in good agreement with those of the Raman analysis, and confirm the high purity of TiO<sub>2</sub> nanospheres. The elemental composition study helps in the identification of inorganic elements present in the materials. Figure 1d presents the different results, and shows the presence of elements such as Cl, Ti and Cu in TiO<sub>2</sub> nanospheres. We have noted a considerable amount of the element Ti in the nanospheres. The presence of the elements Cl and Cu in the TiO<sub>2</sub> nanospheres could be explained by the impurities present in the reagents used in the synthesis of these nanospheres, as the degree of purity of the titanium tetraisopropoxide used was 97%. The formation of TiO<sub>2</sub> is the result of heat treatment during the synthesis process. This result regarding the elemental composition testifies to the successful formation of TiO<sub>2</sub>-NS.

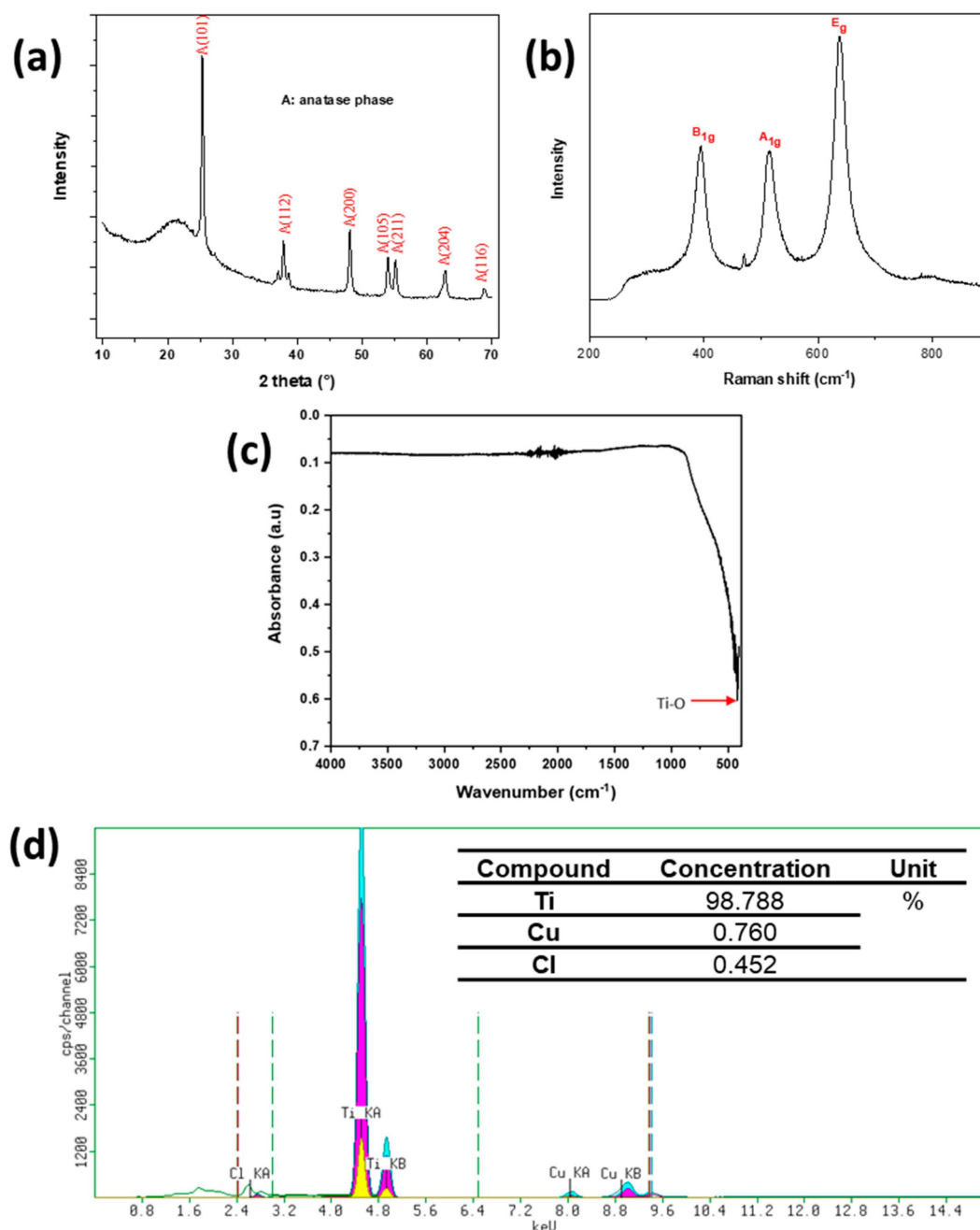


**Figure 1.** (a) XRD diffractogram, (b) Raman spectra, (c) FTIR spectra and (d) Elemental Composition of  $\text{TiO}_2$ -NS.

### 3.1.2. SEM Analysis and Specific Surface Area of $\text{TiO}_2$ -NS

The surface morphologies of the  $\text{TiO}_2$  nanoparticles were examined by scanning electron microscopy (SEM), which revealed that  $\text{TiO}_2$  has a spherical shape with better dispersion (Figure 2). A weak agglomeration of the nanoparticles was also observed, which may be due to the aggregation of the primary  $\text{TiO}_2$  particles at a high calcination temperature, which is necessary to accelerate the crystal growth of the nanoparticles. The BET theory, using the  $\text{N}_2$  adsorption–desorption isotherm, was employed to study the specific surface area (Table 2). According to the BET results,  $\text{TiO}_2$ -NS had a moderate surface area of  $33.3 \text{ m}^2/\text{g}$ , signifying that the  $\text{TiO}_2$ -NS would be able to fix contaminants and facilitate the photocatalytic process.

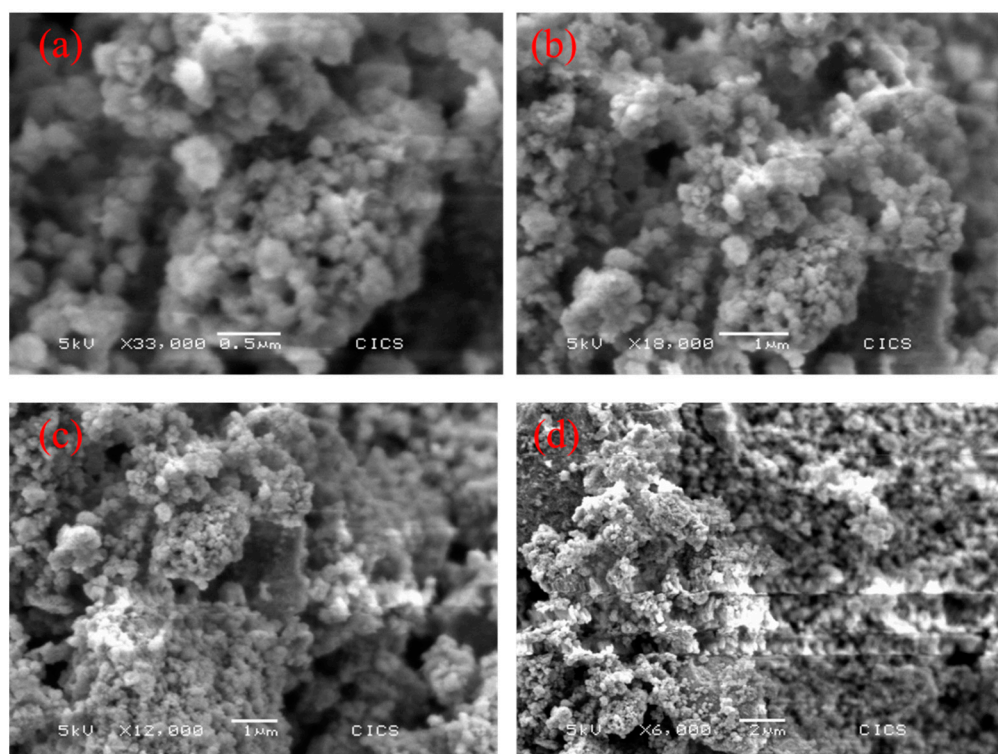


**Figure 2.** SEM images of TiO<sub>2</sub>-NS at different magnifications: (a) ×33,000 (0.5 μm), (b) ×18,000 (1 μm), (c) ×12,000 (1 μm) and (d) ×6000 (2 μm).

**Table 2.** Specific surface area data.

Materials	S <sub>BET</sub> (m <sup>2</sup> /g)	Pore Volume (cm <sup>3</sup> /g)	Pore Size (Å)	Nanoparticle Size (Å)
TiO <sub>2</sub> -NS	33.3	0.2	201.0	470.9

### 3.1.3. UV-Vis Diffuse Reflectance Spectroscopy (DRS)

The optical properties of TiO<sub>2</sub> nanospheres were studied using UV-Vis diffuse reflectance spectra (Figure 3). It can be seen in Figure 3a that TiO<sub>2</sub> nanospheres absorb UV light. As in our previous work, the band gap energy was calculated using the Kubelka–Munk equation [43,44]. Consequently, Figure 3b shows a slight decrease in the bandgap energy of TiO<sub>2</sub>-NS (2.9 eV) compared with that of commercial TiO<sub>2</sub>, as described in the literature, which could be beneficial to photodegradation in the visible range. The activity in the visible range could be explained by the difference in the morphology, surface chemical composition and crystal composition of TiO<sub>2</sub>-NS compared to the commercial and other forms of TiO<sub>2</sub> synthesized differently. It is highly likely that a large number of defects (such as oxygen vacancies, etc.) exist, and lead to a reduction in the bandgap value, resulting in (slight) absorption in the visible range. Similarly, the presence of a small amount of copper, a transition metal, could also explain the activity of TiO<sub>2</sub>-NS in the visible range, as explained in the literature. The literature shows an increase in the bandgap for 3% Cu-doped TiO<sub>2</sub>, corresponding to an 18% enhancement in the efficiency of bare TiO<sub>2</sub> [45]. In addition, 10% Cu-doped TiO<sub>2</sub> enhanced hydrogen generation under irradiation in the visible range by reducing the band gap energy of the material [46].

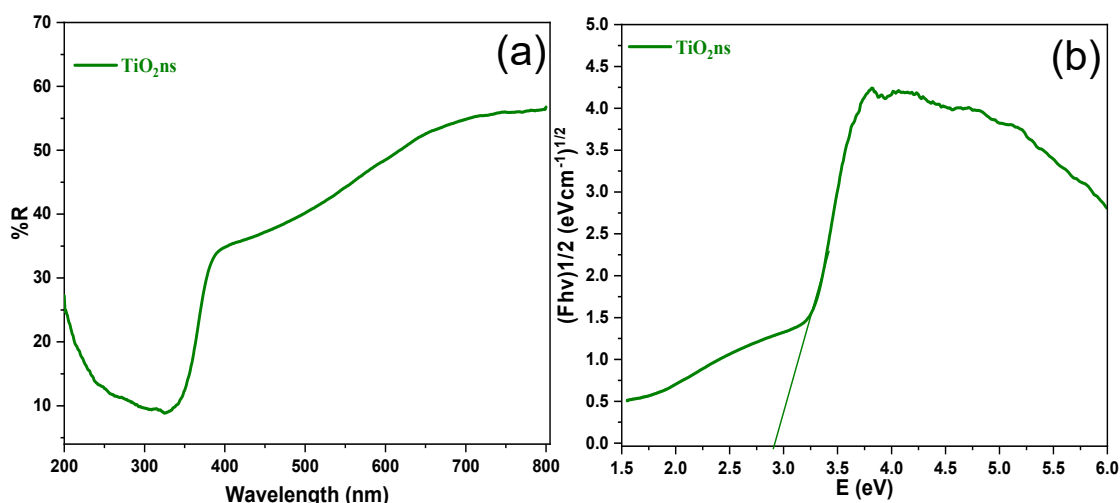


**Figure 3.** (a) Diffuse reflectance spectra and (b) Plot of transferred Kubelka-Munk Versus energy of TiO<sub>2</sub>-NS.

### 3.2. Photocatalytic Activity of TiO<sub>2</sub>-NS under UV and Visible Light

The photocatalytic activity of TiO<sub>2</sub>-NS was evaluated under UV and visible light for the degradation of TTZ at 5 ppm. The degradation efficiencies of the pollutant after 180 min of irradiation are shown in Figure 4. In order to examine the potential role of the photolysis of TTZ, the first experiment was carried out using only UV radiation (in the absence of the photocatalyst). It can be seen that in the absence of TiO<sub>2</sub>-NS, the degradation efficiency remained unchanged with increasing irradiation time (Figure 4), indicating the negligible photolysis of TTZ. In fact, the results show that the catalyst played a crucial role in the photodegradation of TTZ under light irradiation. Indeed, a significant increase in photocatalytic activity was observed due to the presence of TiO<sub>2</sub>-NS. These results also reveal the weak sorption of the dye over a period of 60 min in the dark, with the absorbance of TTZ after adsorption-desorption equilibrium decreasing by 10%. On the other hand, it is worth noting that under UV light, we observed that the degradation efficiency of TTZ reached 100% after 150 min of irradiation, while in the case of visible light exposure, a gradual increase in the degradation efficiency of TTZ as per the degradation efficiency obtained was 57% (Figure 4) after 180 min of irradiation, which demonstrates the ability of TiO<sub>2</sub>-NS to perform photodegradation under visible light. Similar results have been reported on the photocatalytic performance of TiO<sub>2</sub>-NS in the degradation of organic contaminants [47,48]. These results demonstrate that TiO<sub>2</sub>-NS can be excited by visible light for dye degradation purposes.

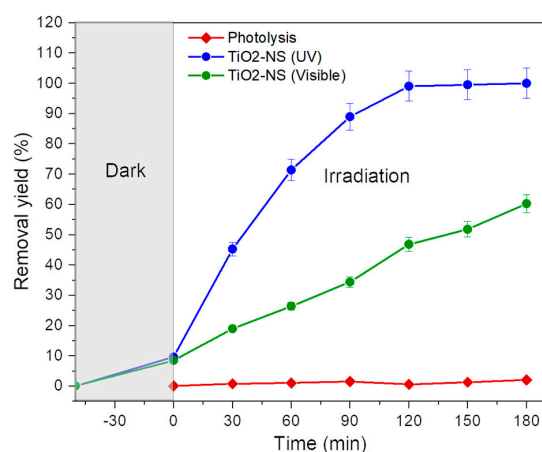


**Figure 4.** Adsorption equilibrium and photocatalytic degradation of tartrazine with TiO<sub>2</sub>-NS catalyst under UV and visible light ( $C_0$ : 5 ppm.  $C_{\text{TiO}_2\text{-NS}}$ : 0.2 g/L. V: 200 mL. natural pH: 6).

### 3.3. Catalyst Dose Effect

The catalyst dosage is a crucial factor in the photocatalytic reaction [49]. Consequently, the effect of TiO<sub>2</sub>-NS dose on the tartrazine photodegradation (at 5 ppm of initial concentration) under visible light irradiation was studied by varying the catalyst concentration from 0.1 g/L to 0.3 g/L. As reflected in Figure 5, the degradation efficiency of tartrazine increases from 52% to 100% when enhancing the photocatalyst concentration from 0.1 g/L to 0.3 g/L, which may be explained by the abundance of active sites on the photocatalyst surface, leading to the generation of a great quantity of ROS ( $\bullet\text{OH}$ ,  $\text{HO}_2\cdot$ ) [50].

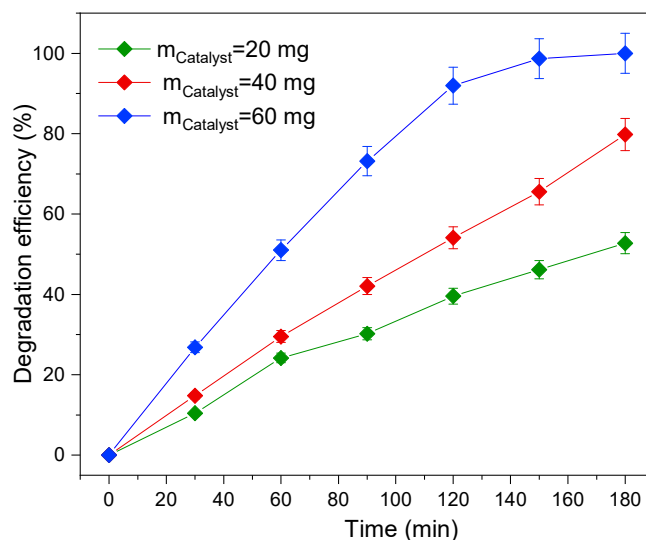


**Figure 5.** Effect of catalyst dose on tartrazine degradation under visible light ( $C_0$ : 5 ppm.  $V_{\text{solution}}$ : 200 mL. Natural pH: 6).

#### 3.3.1. Initial TTZ Concentration Effect and Kinetics of Degradation

The influence of the initial TTZ concentration on degradation was studied for concentrations of 2 to 12 ppm. Figure 6a shows that increasing the dye concentration decreases the photodegradation rate. This can be attributed to the number of active sites available when using the same amount of catalyst for different dye concentrations [51]. With a low initial concentration, TiO<sub>2</sub>-NS produces a sufficient number of active sites for the adsorption of TTZ molecules. With higher initial concentrations, the number of available active sites and the amount of produced ROS are not sufficient for adsorbing/degrading the high number of dye molecules and intermediate products, which reduces the efficiency of dye degradation [52].

The kinetic analysis of TTZ was carried out by determining the rate of pseudo-first-order reaction ( $k$ ) using (Equation (2)) [53].

$$\ln\left(\frac{C_0}{C}\right) = k \times t \quad (2)$$

where  $k$  is the rate of pseudo-first-order reaction ( $\text{min}^{-1}$ ) and  $t$  is the reaction time in min.

The slope of the straight-line  $\ln(C_0/C)$  as a function of time was used to define the value of the pseudo-first-order reaction rate ( $k$ ). As shown in Figure 6b, the  $R^2$  (correlation coefficient) values obtained for TTZ concentrations of 2, 5, 8, and 12 ppm were 0.973, 0.976, 0.999, and 0.972, respectively, demonstrating that the pseudo-first-order kinetic model describes the degradation of TTZ by TiO<sub>2</sub>-NS. We also note that  $k$  increases inversely with contaminant concentration, as has already been documented in previous studies [54]. For the initial TTZ concentration of 2 ppm, the degradation efficiency reaches 100% after 60 min of visible light irradiation, and then there are no kinetics for modeling after this time. Similar behaviors were reported by Zeghioud et al. [55] and Mouhamadou et al. [56].

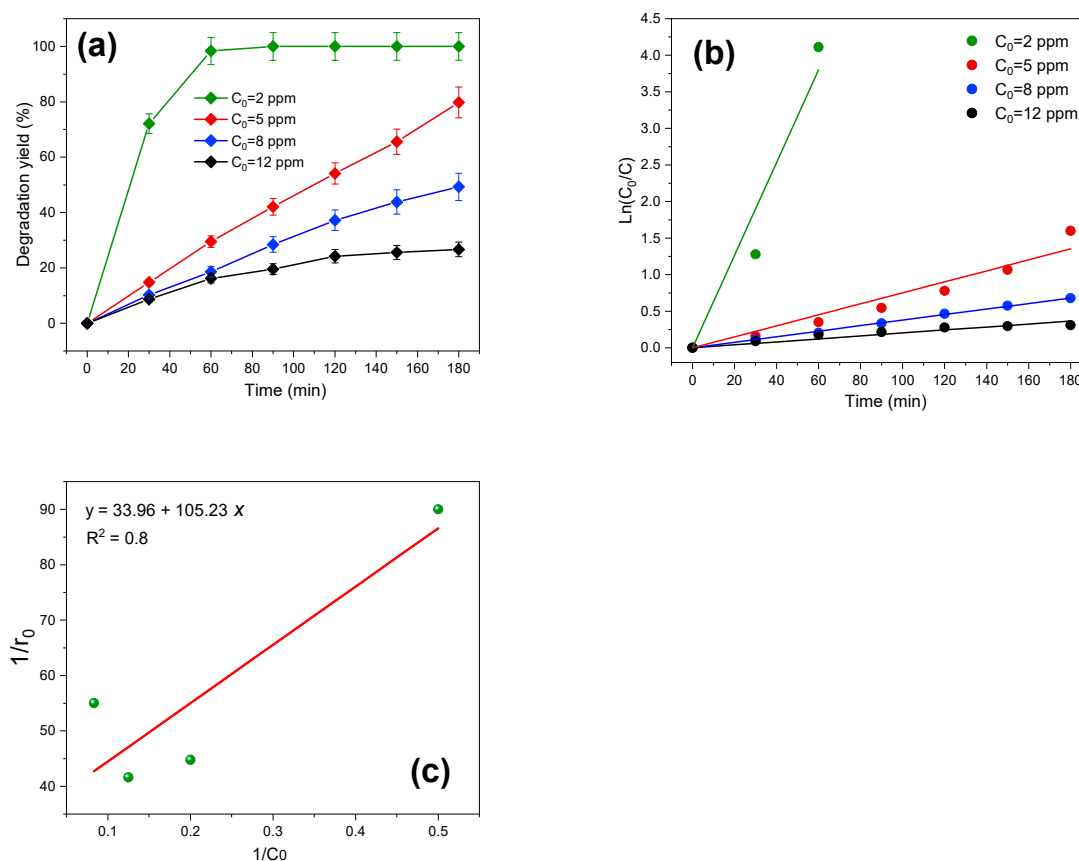


**Figure 6.** (a) Effect of initial Tartrazine concentration with 200 mL of solution and 40 mg of catalyst at natural pH, under visible light irradiation; (b) PFO kinetics for tartrazine degradation under visible light ( $[TTZ]_0 = 2\text{--}12$  ppm.  $V_{\text{solution}}: 200$  mL. Natural pH: 6.  $C_{\text{TiO}_2\text{-NS}}: 0.2$  g/L. Reaction time = 180 min), (c) Langmuir–Hinshelwood plot for photodegradation of tartrazine under visible light ( $[TTZ]_0 = 2\text{--}12$  ppm.  $V_{\text{solution}}: 200$  mL. Natural pH: 6.  $C_{\text{TiO}_2\text{-NS}}: 0.2$  g/L. Reaction time = 180 min).

The photocatalytic degradation reactions of several organic pollutants have been described by the Langmuir–Hinshelwood model (L-H) (Equation (3)) [57], because it takes into consideration the interaction between radicals and substrate molecules that are adsorbed on the surfaces of catalysts throughout the process [55].

$$r_0 = -\frac{dC_0}{dt} = \frac{k \times K \times C_0}{1 + KC_0} \quad (3)$$

where  $r_0$  ( $\text{mg} \cdot \text{min}^{-1} \cdot \text{L}^{-1}$ ) denotes the initial reaction rate,  $k$  ( $\text{mg} \cdot \text{min}^{-1} \cdot \text{L}^{-1}$ ) is the apparent L-H rate and  $K$  ( $\text{L} \cdot \text{mg}^{-1}$ ) is the adsorption/desorption equilibrium constant.

The linearized form of the L-H model is commonly applied to describe the mechanism of heterogenous photocatalytic reactions, according to Equation (4) [58,59].

$$\frac{1}{r_0} = \frac{1}{k \times K \times C_0} + \frac{1}{k} \quad (4)$$

The linear plot of  $\frac{1}{r_0}$  versus  $\frac{1}{C_0}$  (Figure 6c) was used to calculate the constant values of  $k$  and  $K$ , which were discovered to be, respectively,  $0.029 \text{ mg} \cdot \text{min}^{-1} \cdot \text{L}^{-1}$  and  $0.32 \text{ L} \cdot \text{mg}^{-1}$ . As seen in Table 3, these values are significantly lower than those reported in previous studies for organic degradation compounds. This could be explained by the pollutant's high molecular weight, which would slow down the degradation process. Additionally,

this variance in the L-H model's constants may be explained by the source of light used for irradiation and the UV lamp's low intensity value.

**Table 3.** Langmuir–Hinshelwood model constants reported by previous studies related to the organic compound's degradation.

Pollutant	Photocatalyst	Irradiation Source	$k$ ( $\text{mg}\cdot\text{min}^{-1}\cdot\text{L}^{-1}$ )	$K$ ( $\text{L}\cdot\text{mg}^{-1}$ )	Ref.
Acetaminophen	$\text{TiO}_2$	Simulated solar light	0.385	0.0970	[60]
Ciprofloxacin	$\text{CuFe}_2\text{O}_4$	UV-C light irradiation	0.141	0.202	[61]
Acid Red dye	Activated carbon- $\text{TiO}_2$ composite	UV light irradiation	1.78	0.06	[62]
Reactive green 12	$\text{TiO}_2$ loading on polyester	UV light irradiation	0.035	0.796	[55]
Tartrazine	Synthesized $\text{TiO}_2$ -NS	Visible light irradiation	0.029	0.32	This work

### 3.3.2. Effect of pH

pH value is one of the most important parameters influencing the rate of degradation of organic compounds in the photocatalytic process in numerous ways. To study the effect of pH on the degradation efficiency of TTZ and NBB in a binary mixture solution under VL, all experiments were carried out at various pH values, constant initial dye concentrations ( $C_{\text{TTZ}}$ : 2 ppm,  $C_{\text{NBB}}$ : 2.33 ppm) and a  $\text{TiO}_2$  catalyst dosage of 40 mg. The pH of the solution was varied between 2 and 10 by adding the required volume of HCl or NaOH solution. From Figure 7, we can clearly see that the degradation efficiency values of the dyes for different pH increased in the pattern  $\text{pH } 10 < \text{pH } 6 < \text{pH } 2$ . Maximum degradation was yielded at pH 2 for both dyes, with 100% degradation efficiency. At a natural pH of 6 of the binary mixture of TTZ and NBB, the degradation efficiencies of TTZ and NBB were 31% and 50%, respectively. Finally, at pH 10, the degradation efficiencies were the lowest for the two dyes, at 2% for TTZ and 36% for NBB.

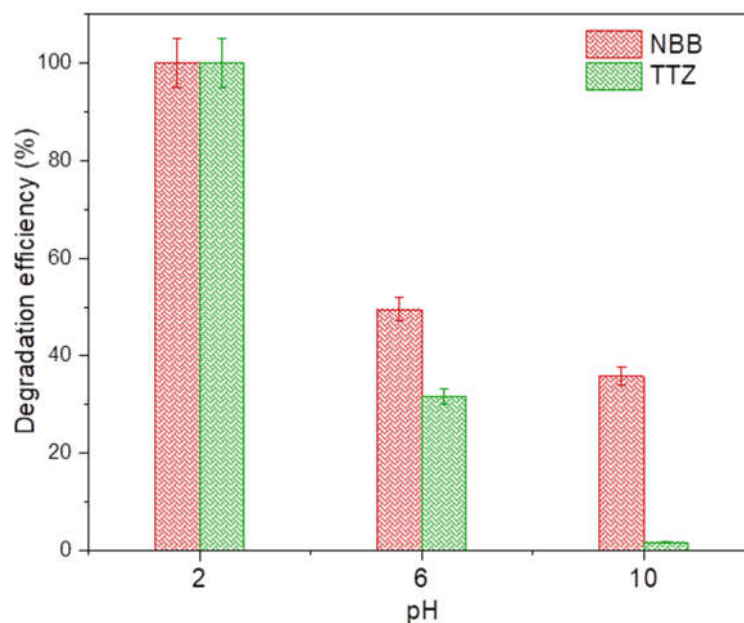
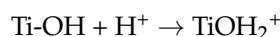


**Figure 7.** Photocatalytic degradation of binary solution of TTZ and NBB with  $\text{TiO}_2$  nanosphere catalyst under visible light at different pH values ( $C_{\text{TTZ}}$ : 2 ppm,  $C_{\text{NBB}}$ : 2.33 ppm,  $C_{\text{TiO}_2\text{-NS}}$ : 0.2 g/L,  $V_{\text{solution}}$ : 200 mL, Treatment duration: 120 min, 10 ppm of NaCl presence).

The pH of the solution influences the charge on the surface of the photocatalyst and also the ionic species of dye in the solution. At an acidic pH, the adsorption of the dye on

the surface of  $\text{TiO}_2$  is higher than that at a neutral or basic pH, which can be attributed to the fact that  $\text{TiO}_2$  shows an amphoteric characteristic [63]. In this case,  $\text{TiO}_2$  has a negatively charged surface at acidic pH, and is positively charged at basic pH [64]. The following equations express the phenomenon [65].

Acidic pH:



Basic pH:



TTZ and NBB are anionic dyes [63,65]; their degradation efficiency increases at acidic pH because of the positive charge of  $\text{TiO}_2$  in the acidic solution. The adsorption and degradation decreased as the pH increased because of the negative charge of  $\text{TiO}_2$  in the basic solution.

### 3.4. Binary System Study

In order to get closer to real conditions, we evaluated the performance of the synthesized  $\text{TiO}_2$ -NS photocatalyst on the simultaneous degradation of two azo dyes, namely, Tartrazine (TTZ) and Naphthol Blue Black (NBB). Indeed, the mixture of dyes most likely to be encountered on an industrial scale is composed of azo dyes, because they represent 60% of commercial dyes [66,67]. As reflected in Figure 8, higher photocatalytic performances were obtained regarding NBB compared to TTZ. Indeed, NBB degradation at 2.33 ppm was 64% (Figure 8b), whereas in the case of TTZ at 2 ppm, it was only 45% (Figure 8a) after 180 min of irradiation. This may be explained by a greater involvement of  $\bullet\text{OH}$  radicals in the case of NBB.

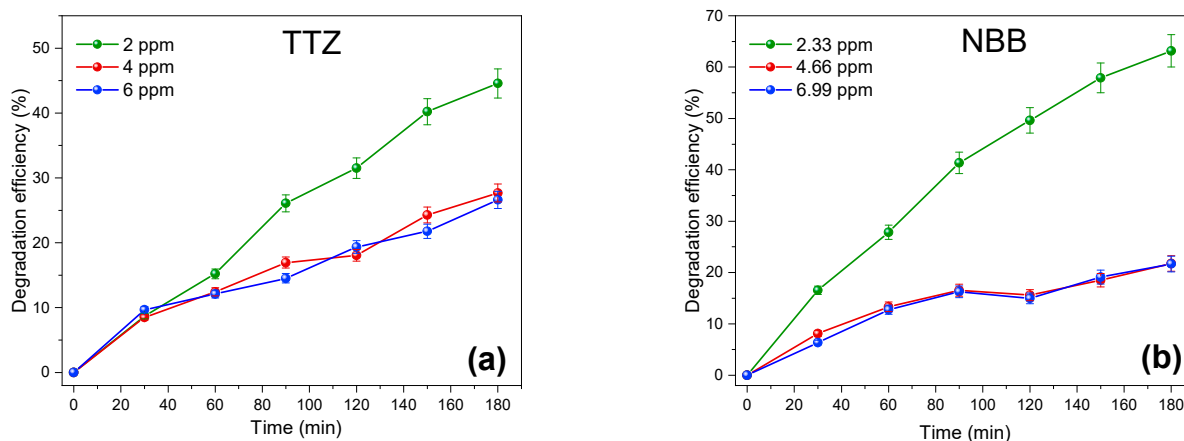


**Figure 8.** (a) Photocatalytic degradation of Tartrazine (TTZ) ( $C_{\text{NBB}}$ : 2.33 ppm.  $m_{\text{TiO}_2\text{-NS}}$ : 40 mg.  $V_{\text{solution}}$ : 200 mL. Natural pH: 6, 10 ppm of NaCl presence) and of (b) Naphthol Blue Black (NBB) ( $C_{\text{TTZ}}$ : 2 ppm.  $m_{\text{TiO}_2\text{-NS}}$ : 40 mg.  $V_{\text{solution}}$ : 200 mL. natural pH: 6, 10 ppm of NaCl presence) in binary solution under visible light.

The degradation efficiency of the dyes decreased with an increase in the initial dye concentration, as observed in Figure 8. Additionally, this also indicates that higher initial concentrations of TTZ (4 ppm, 6 ppm) and NBB (4.66 ppm, 6.99 ppm) resulted in degradation efficiencies of approximately 22% and 27%, respectively. This may be due to the reduced generation of radical species on the surface of the photocatalyst. The amount of dye that saturates the surface of the photocatalyst is important for photodegradation; as the active sites on the  $\text{TiO}_2$ -NS photocatalyst become occupied by dye molecules, the generation of  $\bullet\text{OH}$  radicals on the surface of the photocatalyst decreases [68,69]. As the concentration

of dye molecules increases, fewer photons reach the catalyst surface of TiO<sub>2</sub>-NS, thereby reducing the formation of •OH and decreasing the photodegradation efficiency [70].

### 3.5. Experimental Design Results

#### 3.5.1. Optimization of Parameters Using Response Surface Methodology (RSM)

The design of experiments offers a systematic approach to distinguishing the importance of certain variables to the results, their interactions, and the effects of controlling them on achieving the optimal response [71]. To determine the relationship between the various experimental parameters and the results obtained, response surface methodology (RSM) is one of the most widely used empirical modeling techniques for the multivariate optimization of experimental results [56,72]. The RSM was used to analyze and optimize the photocatalytic degradation of TTZ and NBB using TiO<sub>2</sub> nanospheres. For this study, 13 trials were performed, and the degradation removal rates are presented in Table 4. The degradation efficiencies ranged from 15.38% to 44.55% (TTZ) and from 21.75% to 63.14% (NBB).

**Table 4.** Experimental design to assess the mutual effects of second pollutant presence and NaCl on the photocatalytic degradation TTZ and NBB.

Run	Factor 1	Factor 2	Factor 3	Response 1	Response 2
	A: C <sub>TTZ</sub> (ppm)	B: C <sub>NBB</sub> (ppm)	C: C <sub>NaCl</sub> (ppm)	Degradation Yield TZ (%)	Degradation Yield NBB (%)
1	2	2.33	10	44.55	63.14
2	2	2.33	6	32.97	52.71
3	3	3.495	10	15.94	30.2
4	2	2.33	2	44.32	60.31
5	4	2.33	2	25	38.06
6	2	4.66	6	15.38	22.33
7	4	2.33	6	26.44	32
8	4	2.33	10	27.68	37.74
9	3	3.495	6	18.37	30.33
10	3	3.495	2	22.82	34.74
11	2	4.66	10	16.15	21.75
12	2	4.66	2	20.61	28.99
13	3	3.495	6	18.79	28.09

On the basis of the experimental data presented in Table 4, a polyfunctional equation describing the photodegradation process was established, expressed as follows (Equations (5) and (6)):

$$(\text{Degradation yield TTZ} + 17)^{-1.83} = -0.0019 + 0.0007C_{\text{TTZ}} + 0.0005C_{\text{NBB}} + 0.0005C_{\text{NaCl}} - 0.0001C_{\text{TTZ}} \times C_{\text{NBB}} - 0.0002C_{\text{TTZ}} \times C_{\text{NaCl}} - 6 \times 10^{-5}C_{\text{NBB}} \times C_{\text{NaCl}} - 3 \times 10^{-5}C_{\text{NaCl}}^2 + 4 \times 10^{-5}C_{\text{TTZ}} \times C_{\text{NBB}} \times C_{\text{NaCl}} + 8 \times 10^{-6}C_{\text{TTZ}} \times C_{\text{NaCl}}^2. \quad (5)$$

$$(\text{Degradation yield NBB})^{0.3} = 4899 - 0.311C_{\text{TTZ}} - 0.383C_{\text{NBB}} - 0.112C_{\text{NaCl}} + 0.043C_{\text{TTZ}} \times C_{\text{NBB}} - 0.003C_{\text{TTZ}} \times C_{\text{NaCl}} + 0.007C_{\text{NBB}} \times C_{\text{NaCl}} + 0.013C_{\text{NaCl}}^2 - 0.002C_{\text{NBB}} \times C_{\text{NaCl}}^2. \quad (6)$$

This empirical linear regression (Equations (5) and (6)) provides clear information on the positive or negative effects of the main variables, while the numerical coefficient is related to the significance of the effect. It is clear from Equations (5) and (6) that the TTZ concentration plays the most important role in the process, followed by the NBB concentration, and finally the NaCl concentration. To validate the model, an analysis of variance (ANOVA) was applied, the results of which are presented in Tables 5 and 6. The statistical significance of the model is attributed to the F value [73]. F values of 110 (TTZ) and 193.93 (NBB) imply that the model is highly significant. There are only 0.13% (TTZ)

and 0.01% (NBB) chances that an F value of this magnitude is due to noise [74,75]. The very low probability values of  $p$ -value  $< 0.0013$  (TTZ) and  $p$ -value  $< 0.0001$  (NBB) confirm that the model is highly significant at the 95% confidence level. According to Sohrabi and Shahnaz, a model is significant when the  $p$ -value is  $< 0.05$  [73,76].

**Table 5.** ANOVA table and fit statistics of Tartrazine degradation.

Source	Sum of Squares	df	Mean Square	F-Value	$p$ -Value	
Model	$2.001 \times 10^{-6}$	9	$2.224 \times 10^{-7}$	110.00	0.0013	Significant
A-C <sub>TTZ</sub>	$9.303 \times 10^{-8}$	1	$9.303 \times 10^{-8}$	46.02	0.0065	
B-C <sub>NBB</sub>	$8.724 \times 10^{-7}$	1	$8.724 \times 10^{-7}$	431.59	0.0002	
C-C <sub>NaCl</sub>	$1.199 \times 10^{-7}$	1	$1.199 \times 10^{-7}$	59.29	0.0046	
AB	$4.421 \times 10^{-8}$	1	$4.421 \times 10^{-8}$	21.87	0.0185	
AC	$3.440 \times 10^{-8}$	1	$3.440 \times 10^{-8}$	17.02	0.0258	
BC	$1.004 \times 10^{-7}$	1	$1.004 \times 10^{-7}$	49.65	0.0059	
C <sup>2</sup>	$2.006 \times 10^{-8}$	1	$2.006 \times 10^{-8}$	9.92	0.0513	
ABC	$4.730 \times 10^{-8}$	1	$4.730 \times 10^{-8}$	23.40	0.0168	
AC <sup>2</sup>	$3.452 \times 10^{-8}$	1	$3.452 \times 10^{-8}$	17.07	0.0257	
Residual	$6.064 \times 10^{-9}$					
R <sup>2</sup>	0.9970					
Adjusted R <sup>2</sup>	0.9879	3	$2.021 \times 10^{-9}$			
Predicted R <sup>2</sup>	0.7922					
Adeq Precision	29.6421					

**Table 6.** ANOVA table and fit statistics of Naphthol Blue Black degradation.

Source	Sum of Squares	df	Mean Square	F-Value	$p$ -Value	
Model	1.11	8	0.1389	193.93	$< 0.0001$	Significant
A-C tartrazine	0.0780	1	0.0780	108.87	0.0005	
B-C NBB	0.1623	1	0.1623	226.57	0.0001	
C-C NaCl	0.0208	1	0.0208	29.09	0.0057	
AB	0.0059	1	0.0059	8.17	0.0460	
AC	0.0008	1	0.0008	1.18	0.3388	
BC	0.0206	1	0.0206	28.77	0.0058	
C <sup>2</sup>	0.0339	1	0.0339	47.36	0.0023	
BC <sup>2</sup>	0.0022	1	0.0022	3.02	0.1573	
Residual	0.0029	4	0.0007			
R <sup>2</sup>	0.9974					
Adjusted R <sup>2</sup>	0.9923					
Predicted R <sup>2</sup>	0.9805					
Adeq Precision	42.6727					

The values of the R<sup>2</sup>, adjusted R<sup>2</sup> and predicted R<sup>2</sup> coefficients of the applied Box Behnken Design (BBD) model were 0.9970, 0.9879, and 0.7922 (TTZ) and 0.9974, 9923, and 9805 (NBB), respectively (Tables 5 and 6). These R<sup>2</sup> values correspond to the level of agreement between the degradation rates obtained experimentally and those predicted by the proposed model, as shown in Figure 9. The adequate accuracies, which measure the signal-to-noise ratio, are 29.6421 (TTZ) and 42.6727 (NBB), which are well above the lowest acceptable value of 4. This practically means that the proposed model can be safely used to navigate the design region, within the limit of the variables determined previously (Table 4).

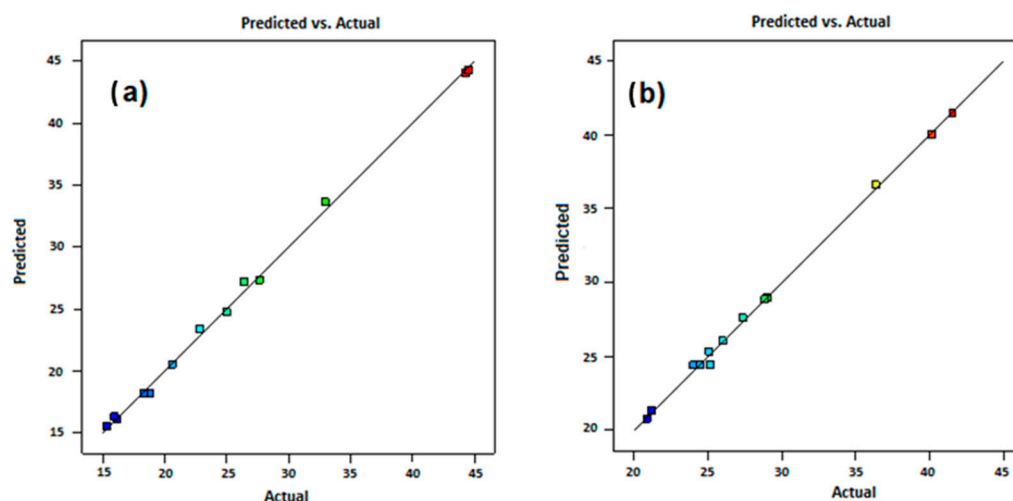


**Figure 9.** Predicted vs. experimental results of degradation efficiency in binary system: (a) Tartrazine; (b) Naphthol Blue Black.

### 3.5.2. Response Surface 3D Graph and Contour Plots of the Interactive Effects

The 3D response surfaces and contours are graphical representations of the regression equation applied for optimizing the reaction conditions, and represent a very useful approach to revealing the factors affecting the reaction system. The results obtained from the combined interaction of three factors are shown in Figure 10 (TTZ) and Figure 11 (NBB).

Figures 10a and 11a show the simultaneous influences of TTZ concentration and NBB concentration on the photodegradation of TTZ and NBB, respectively. As can be seen from the graphs, the interactive effects of TTZ concentration and NBB concentration on both TTZ and NBB removal reveal an exponential response surface. Furthermore, the combined effects of the factors suggest that TTZ and NBB removal rates decrease with increasing concentrations. The corresponding contour plots (Figure 10a) were applied to facilitate a better understanding of the information relating to the interaction effect of the factors on the response. The green region tending towards yellow on the graph indicates maximum degradation.

Figures 10b and 11b show the combined effects of TTZ concentration and NaCl salt interference on TTZ and NBB dye removal. It is evident that the percentage removal of TTZ and NBB exhibits an exponential response surface. The rate of photodegradation is high at low NaCl concentrations for both dyes, as shown in Figures 10c and 11c. These results show that the response increases with decreasing dye and NaCl concentrations in the medium. The corresponding contour plots (Figures 10b,c and 11b,c) give greater visibility to the factors influencing the response. The green area of the contour corresponds to a high percentage of elimination.

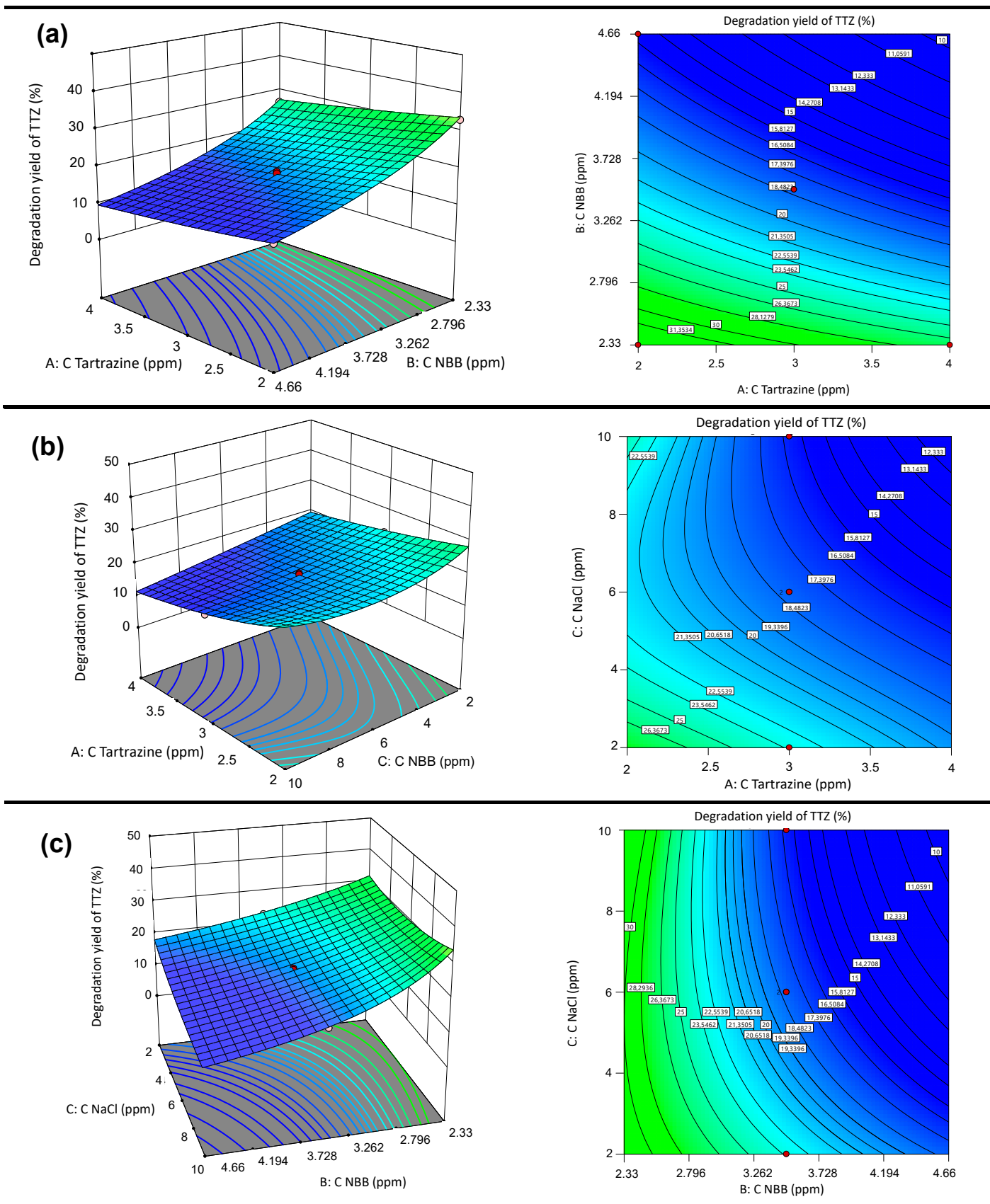


**Figure 10.** RSM surfaces plots and 2D contour plots of the interaction effects between: (a) TTZ and NBB concentrations; (b) TTZ and NaCl concentrations and (c) NaCl and NBB concentrations.

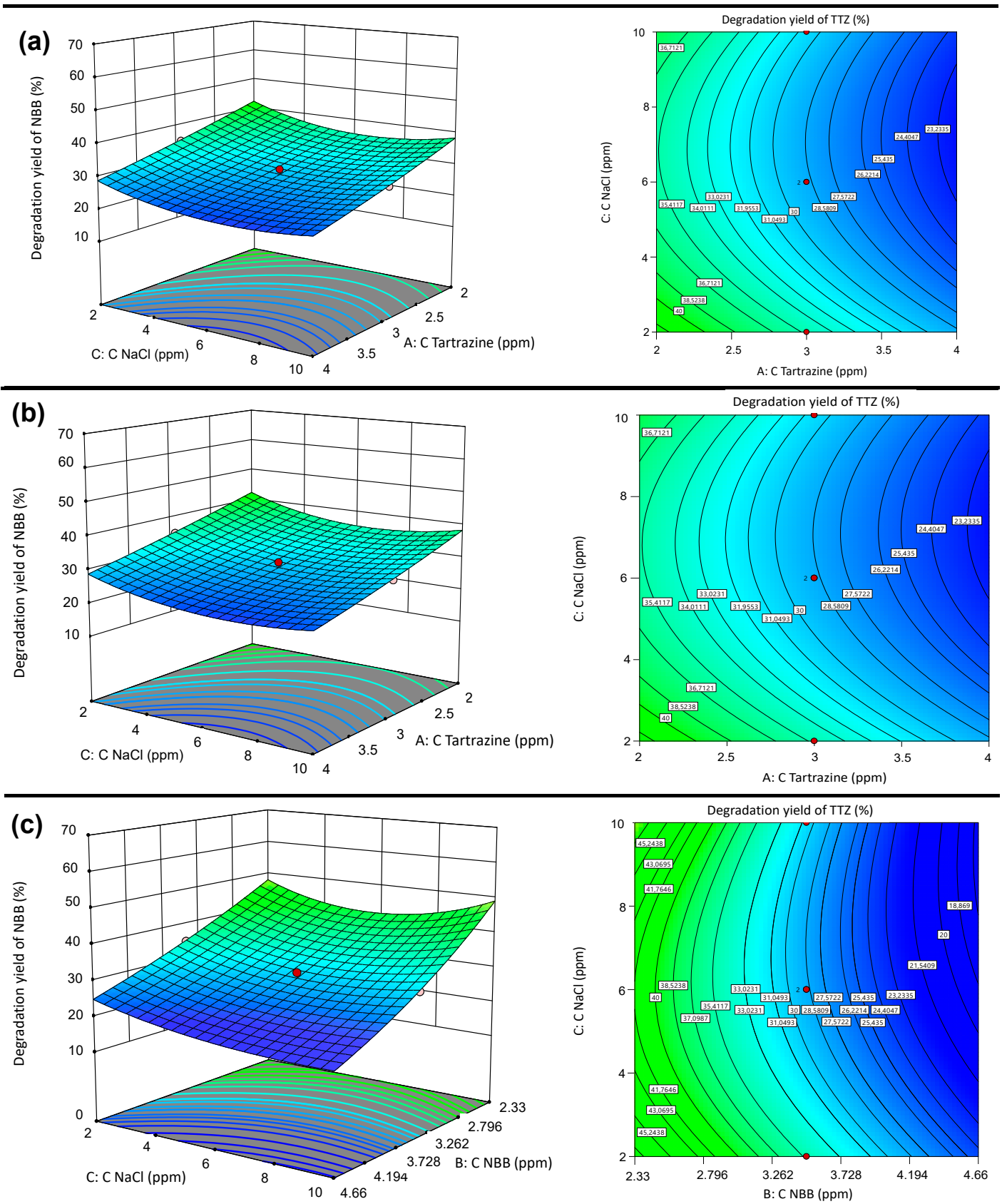


**Figure 11.** RSM surfaces plots and 2D contour plots of the interaction effects between (a) NBB and TTZ concentrations; (b) NaCl and Tartrazine concentrations; and (c) NBB and NaCl concentrations.

### 3.6. Mineralization

In order to evaluate TTZ mineralization in the presence of the synthesized TiO<sub>2</sub>-NS photocatalyst, the TOC removal yields were determined. The degradation efficiency and mineralization yield of TTZ versus the irradiation time are depicted in Figure 12. As can be seen in this last figure, the mineralization results obtained confirm the trend observed relating to contaminant degradation. Indeed, both degradation and mineralization yields increase with irradiation time. Obviously, the degradation of almost all total organic pollutants happens promptly, while TOC drops by only ~31% after 1 h of light exposure, which clearly shows the creation of intermediate transformation products [77,78]. On the other hand, in this study, a highly satisfying mineralization yield was obtained after 180 min, representing 53%. However, a longer irradiation time is necessary to reach the complete mineralization of the pollutant. Although further analysis is required to identify intermediate products, the overall mechanism remains as follows:

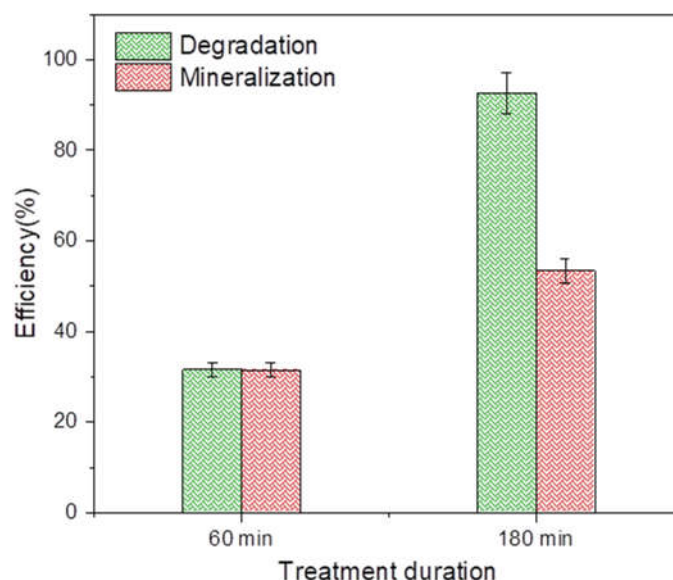
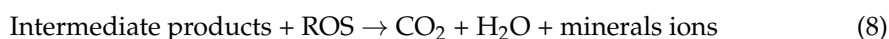
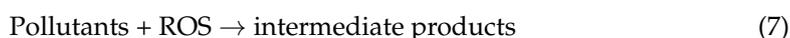


**Figure 12.** Mineralization of tartrazine with TiO<sub>2</sub> nanosphere catalyst under visible light ( $C_0$ : 6 ppm.  $C_{\text{TiO}_2\text{-NS}}$ : 0.2 g/L.  $V_{\text{solution}}$ : 200 mL. Natural pH: 6).

### 3.7. Reuse Test of Photocatalyst

The reusability of the photocatalyst is a crucial factor from both environmental and financial perspectives [57]. In order to examine this parameter, TiO<sub>2</sub>-NS underwent three cycles of photocatalysis under the same operating conditions (TTZ concentration, photocatalyst dosage, and irradiation source). As can be seen in Figure 13, in the third cycle, the pollutant degradation decreased. The loss of photocatalyst active sites, the loss of matter during handling and physical solicitation, and irreversible chemical adsorption could explain the diminution in photoactivity of synthesized materials observed after each cycle [23]. After a certain number of cycles, the photocatalyst would not be reusable, but it has the advantage of being simple to synthesize, as well as inexpensive.

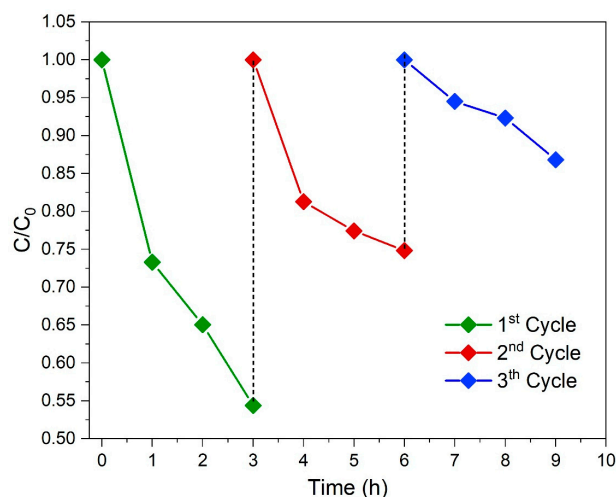


**Figure 13.** Reusability cycles of TiO<sub>2</sub>-NS for photocatalytic degradation of tartrazine under visible light (C<sub>0</sub>: 6 ppm, m<sub>TiO<sub>2</sub>-NS</sub>: 100 mg, V<sub>solution</sub>: 200 mL, natural pH: 6).

#### 4. Conclusions

The structural modification of TiO<sub>2</sub> is a promising route that can lead to a photocatalyst active in the visible range, which can be used in water treatment. The photocatalytic efficiency of TiO<sub>2</sub> nanospheres used in the removal of TTZ dye has been successfully demonstrated. Characterization techniques provide information on surface chemistry and inorganic constituents (FTIR, XRF), crystallinity (Raman spectroscopy), morphology (SEM), specific surface area (BET), and band gap energy (DRS). The experimental data from the pseudo-first-order kinetic model best describe the degradation of TTZ by TiO<sub>2</sub>-NS. The optimized parameters obtained by RSM provide a better understanding of the combined effects of the factors in the reaction system in achieving optimum photodegradation process. Optimization using response surface methodology indicates that pollutant concentration is the most important factor, while NaCl salt interference had a much smaller effect on the photodegradation of the dyes TTZ and NBB. The analysis of variance in the BBD showed good statistical results and provided an effective model for the reaction system. The TiO<sub>2</sub> nanospheres developed showed satisfactory performance in the removal of TTZ and NBB dyes by photocatalysis in the visible range. This study has identified a material that is effective in removing organic contaminants from wastewater. Consequently, its characteristics and qualities make it a suitable photocatalyst for wastewater treatment to remove contaminants.

**Author Contributions:** Conceptualization, S.D. and A.K.; methodology, H.Z.; software, A.A.; validation, P.B., S.D. and H.Z.; formal analysis, C.C.; investigation, B.T.; resources, F.H.; data curation, H.Z.; writing—original draft preparation, F.H.; writing—review and editing, S.D.; visualization, A.A.; supervision, P.B.; project administration, A.K.; funding acquisition, A.K. All authors have read and agreed to the published version of the manuscript.

**Funding:** The authors would like to acknowledge the Erasmus+ International Credit Mobility for the Grant (Grant agreement number: 2019-1-FR01-KA107-060920) between UniLaSalle Polytechnic Institute and University of Maroua. This work was supported by the International Research Center “Innovation Transportation and Production Systems” of the I-SITE CAP 20-25.

**Data Availability Statement:** Data are contained within the article.

**Acknowledgments:** The authors would like to thank Ivane LELIEVRE for her technical help and Marie-Anne Hairan for meticulously proofreading the English language of this paper (UniLaSalle-Ecole des Metiers de l’Environnement de Rennes). The authors thank Christelle Blavignac, Centre Imagerie Cellulaire Sante—UCA PARTNER, for her technical support and expertise.

**Conflicts of Interest:** The authors declare no conflict of interest.

## References

1. Patil, N.S.; Chetan, N.L.; Nataraja, M.; Suthar, S. Climate change scenarios and its effect on groundwater level in the Hiranyakeshi watershed, Groundw. *Sustain. Dev.* **2020**, *10*, 100323. [[CrossRef](#)]
2. Adimalla, N.; Qian, H. Groundwater quality evaluation using water quality index (WQI) for drinking purposes and human health risk (HHR) assessment in an agricultural region of Nanganur, south India. *Ecotoxicol. Environ. Saf.* **2019**, *176*, 153–161. [[CrossRef](#)] [[PubMed](#)]
3. Xia, L.; Zhang, K.; Wang, X.; Guo, Q.; Wu, Y.; Du, Y.; Zhang, L.; Xia, J.; Tang, H.; Zhang, X.; et al. 0D/2D Schottky junction synergies with 2D/2D S-scheme heterojunction strategy to achieve uniform separation of carriers in 0D/2D/2D quasi CN-QDs/TCN/ZnIn<sub>2</sub>S<sub>4</sub> towards photocatalytic remediating petroleum hydrocarbons polluted marine. *Appl. Catal. B Environ.* **2023**, *325*, 122387. [[CrossRef](#)]
4. Zubair, M.; Aziz, H.A.; Ihsanullah, I.; Ahmad, M.A.; Al-Harhi, M.A. Biochar supported CuFe layered double hydroxide composite as a sustainable adsorbent for efficient removal of anionic azo dye from water. *Environ. Technol. Innov.* **2021**, *23*, 101614. [[CrossRef](#)]
5. Rodriguez-Narvaez, O.M.; Peralta-Hernandez, J.M.; Goonetilleke, A.; Bandala, E.R. Treatment technologies for emerging contaminants in water: A review. *Chem. Eng. J.* **2017**, *323*, 361–380. [[CrossRef](#)]
6. Gogoi, A.; Mazumder, P.; Tyagi, V.K.; Chaminda, G.G.T.; An, A.K.; Kumar, M. Occurrence and fate of emerging contaminants in water environment: A review. *Groundw. Sustain. Dev.* **2018**, *6*, 169–180. [[CrossRef](#)]
7. Xia, L.; Sun, Z.; Wu, Y.; Yu, X.-F.; Cheng, J.; Zhang, K.; Sarina, S.; Zhu, H.-Y.; Weerathunga, H.; Zhang, L.; et al. Leveraging doping and defect engineering to modulate exciton dissociation in graphitic carbon nitride for photocatalytic elimination of marine oil spill. *Chem. Eng. J.* **2022**, *439*, 135668. [[CrossRef](#)]
8. De Lima Barizão, A.C.; Silva, M.F.; Andrade, M.; Brito, F.C.; Gomes, R.G.; Bergamasco, R. Green synthesis of iron oxide nanoparticles for tartrazine and bordeaux red dye removal. *J. Environ. Chem. Eng.* **2020**, *8*, 103618. [[CrossRef](#)]
9. Dalhatou, S.; Pétrier, C.; Laminsi, S.; Baup, S. Sonochemical removal of naphthol blue black azo dye: Influence of parameters and effect of mineral ions. *Int. J. Environ. Sci. Technol.* **2015**, *12*, 35–44. [[CrossRef](#)]
10. Dalhatou, S.; Laminsi, S.; Pétrier, C.; Baup, S. Competition in sonochemical degradation of Naphthol Blue Black: Presence of an organic (nonylphenol) and a mineral (bicarbonate ions) matrix. *J. Environ. Chem. Eng.* **2019**, *7*, 102819. [[CrossRef](#)]
11. Perveen, S.; Nadeem, R.; Nosheen, F.; Asjad, M.I.; Awrejcewicz, J.; Anwar, T. Biochar-Mediated Zirconium Ferrite Nanocomposites for Tartrazine Dye Removal from Textile Wastewater. *Nanomaterials* **2022**, *12*, 2828. [[CrossRef](#)] [[PubMed](#)]
12. Nemiwal, M.; Zhang, T.C.; Kumar, D. Recent progress in g-C<sub>3</sub>N<sub>4</sub>, TiO<sub>2</sub> and ZnO based photocatalysts for dye degradation: Strategies to improve photocatalytic activity. *Sci. Total Environ.* **2021**, *767*, 144896. [[CrossRef](#)] [[PubMed](#)]
13. Ichipi, E.O.; Tichapondwa, S.M.; Chirwa, E.M.N. Plasmonic effect and bandgap tailoring of Ag/Ag<sub>2</sub>S doped on ZnO nanocomposites for enhanced visible-light photocatalysis. *Adv. Powder Technol.* **2022**, *33*, 103596. [[CrossRef](#)]
14. Kanakaraju, D.; Glass, B.D.; Oelgemöller, M. Advanced oxidation process-mediated removal of pharmaceuticals from water: A review. *J. Environ. Manag.* **2018**, *219*, 189–207. [[CrossRef](#)]
15. Olmez-Hanci, T.; Arslan-Alaton, I. Comparison of sulfate and hydroxyl radical based advanced oxidation of phenol. *Chem. Eng. J.* **2013**, *224*, 10–16. [[CrossRef](#)]
16. Guaraldo, T.T.; Wenk, J.; Mattia, D. Photocatalytic ZnO Foams for Micropollutant Degradation. *Adv. Sustain. Syst.* **2021**, *5*, 2000208. [[CrossRef](#)]
17. Zhu, D.; Zhou, Q. Action and mechanism of semiconductor photocatalysis on degradation of organic pollutants in water treatment: A review, *Environ. Nanotechnology. Monit. Manag.* **2019**, *12*, 100255. [[CrossRef](#)]
18. Sharma, K.; Raizada, P.; Hasija, V.; Singh, P.; Bajpai, A.; Nguyen, V.H.; Rangabhashiyam, S.; Kumar, P.; Nadda, A.K.; Kim, S.Y.; et al. ZnS-based quantum dots as photocatalysts for water purification. *J. Water Process Eng.* **2021**, *43*, 102217. [[CrossRef](#)]
19. Sajid, M.M.; Shad, N.A.; Javed, Y.; Khan, S.B.; Zhang, Z.; Amin, N.; Zhai, H. Preparation and characterization of Vanadium pentoxide (V<sub>2</sub>O<sub>5</sub>) for photocatalytic degradation of monoazo and diazo dyes. *Surf. Interfaces* **2020**, *19*, 100502. [[CrossRef](#)]
20. Hitam, C.N.C.; Jalil, A.A. A review on exploration of Fe<sub>2</sub>O<sub>3</sub> photocatalyst towards degradation of dyes and organic contaminants. *J. Environ. Manag.* **2020**, *258*, 110050. [[CrossRef](#)]
21. Goktas, S.; Goktas, A. A comparative study on recent progress in efficient ZnO based nanocomposite and heterojunction photocatalysts: A review. *J. Alloys Compd.* **2021**, *863*, 158734. [[CrossRef](#)]
22. Paumo, H.K.; Dalhatou, S.; Katata-Seru, L.M.; Kamdem, B.P.; Tijani, J.O.; Vishwanathan, V.; Kane, A.; Bahadur, I. TiO<sub>2</sub> assisted photocatalysts for degradation of emerging organic pollutants in water and wastewater. *J. Mol. Liq.* **2021**, *331*, 115458. [[CrossRef](#)]
23. Hsu, C.-Y.; Mahmoud, Z.H.; Abdullaev, S.; Ali, F.K.; Naeem, Y.A.; Mizher, R.M.; Karim, M.M.; Abdulwahid, A.S.; Ahmadi, Z.; Habibzadeh, S.; et al. Nano titanium oxide (nano-TiO<sub>2</sub>): A review of synthesis methods, properties, and applications. *Case Stud. Chem. Environ. Eng.* **2024**, *9*, 100626. [[CrossRef](#)]
24. Pelaez, M.; Nolan, N.T.; Pillai, S.C.; Seery, M.K.; Falaras, P.; Kontos, A.G.; Dunlop, P.S.M.; Hamilton, J.W.J.; Byrne, J.A.; O'Shea, K.; et al. A review on the visible light active titanium dioxide photocatalysts for environmental applications. *Appl. Catal. B Environ.* **2012**, *125*, 331–349. [[CrossRef](#)]
25. Al Zoubi, W.; Al-Hamdani, A.A.S.; Sunghun, B.; Ko, Y.G. A review on TiO<sub>2</sub>-based composites for superior photocatalytic activity. *Rev. Inorg. Chem.* **2021**, *41*, 213–222. [[CrossRef](#)]

26. Ibhaddon, A.O.; Fitzpatrick, P. Heterogeneous photocatalysis: Recent advances and applications. *Catalysts* **2013**, *3*, 189–218. [[CrossRef](#)]
27. Karthigadevi, G.; Manikandan, S.; Karmegam, N.; Subbaiya, R.; Chozhavendhan, S.; Ravindran, B.; Chang, S.W.; Awasthi, M.K. Chemico-nanotreatment methods for the removal of persistent organic pollutants and xenobiotics in water—A review. *Bioresour. Technol.* **2021**, *324*, 124678. [[CrossRef](#)]
28. Nyamukamba, P.; Okoh, O.; Mungondori, H.; Taziwa, R.; Zinya, S. Synthetic Methods for Titanium Dioxide Nanoparticles: A Review. In *Titanium Dioxide-Material for a Sustainable Environment*; IntechOpen: Rijeka, Croatia, 2018. [[CrossRef](#)]
29. Irshad, M.A.; Nawaz, R.; Rehman, M.Z.U.; Adrees, M.; Rizwan, M.; Ali, S.; Ahmad, S.; Tasleem, S. Synthesis, characterization and advanced sustainable applications of titanium dioxide nanoparticles: A review. *Ecotoxicol. Environ. Saf.* **2021**, *212*, 111978. [[CrossRef](#)] [[PubMed](#)]
30. Gupta, T.; Samriti; Cho, J.; Prakash, J. Hydrothermal synthesis of TiO<sub>2</sub> nanorods: Formation chemistry, growth mechanism, and tailoring of surface properties for photocatalytic activities. *Mater. Today Chem.* **2021**, *20*, 100428. [[CrossRef](#)]
31. Guo, W.; Zhang, F.; Lin, C.; Wang, Z.L. Direct growth of TiO<sub>2</sub> nanosheet arrays on carbon fibers for highly efficient photocatalytic degradation of methyl orange. *Adv. Mater.* **2012**, *24*, 4761–4764. [[CrossRef](#)]
32. Konni, M.; Dwarapureddi, B.K.; Dash, S.; Raj, A.; Karnena, M.K. Titanium dioxide electrospun nanofibers for dye removal-A review. *J. Appl. Nat. Sci.* **2022**, *14*, 450–458. [[CrossRef](#)]
33. Shehab, M.A.; Sharma, N.; Valsesia, A.; Karacs, G.; Kristály, F.; Koós, T.; Leskó, A.K.; Nánai, L.; Hernadi, K.; Németh, Z. Preparation and photocatalytic performance of TiO<sub>2</sub> nanowire-based self-supported hybrid membranes. *Molecules* **2022**, *27*, 2951. [[CrossRef](#)] [[PubMed](#)]
34. Assadi, A.A.; Karoui, S.; Trabelsi, K.; Hajjaji, A.; Elfalleh, W.; Ghorbal, A.; Maghzaoui, M.; Assadi, A.A. Performance for Wastewater Treatment under Visible Light. *Materials* **2022**, *15*, 1463. [[CrossRef](#)] [[PubMed](#)]
35. Huang, D.; Liu, H.; Bian, J.; Li, T.; Huang, B.; Niu, Q. High Specific Surface Area TiO<sub>2</sub> Nanospheres for Hydrogen Production and Photocatalytic Activity. *J. Nanosci. Nanotechnol.* **2019**, *20*, 3217–3224. [[CrossRef](#)] [[PubMed](#)]
36. Srinivasan, M.; White, T. Degradation of Methylene Blue by Three-Dimensionally Ordered Macroporous Titania. *Environ. Sci. Technol.* **2007**, *41*, 4405–4409. [[CrossRef](#)] [[PubMed](#)]
37. Wang, X.; Caruso, R.A. Enhancing photocatalytic activity of titania materials by using porous structures and the addition of gold nanoparticles. *J. Mater. Chem.* **2011**, *21*, 20–28. [[CrossRef](#)]
38. Pugazhenthiran, N.; Murugesan, S.; Valdés, H.; Selvaraj, M.; Sathishkumar, P.; Smirniotis, P.G.; Anandan, S.; Mangalaraja, R.V. Photocatalytic oxidation of ceftiofur sodium under UV-visible irradiation using plasmonic porous Ag-TiO<sub>2</sub> nanospheres. *J. Ind. Eng. Chem.* **2022**, *105*, 384–392. [[CrossRef](#)]
39. Haider, A.J.; Al-Anbari, R.H.; Kadhim, G.R.; Salame, C.T. Exploring potential Environmental applications of TiO<sub>2</sub> Nanoparticles. *Energy Procedia* **2017**, *119*, 332–345. [[CrossRef](#)]
40. Askari, M.B.; Banizi, Z.T.; Seifi, M.; Dehaghi, S.B.; Veisi, P. Synthesis of TiO<sub>2</sub> nanoparticles and decorated multi-wall carbon nanotube (MWCNT) with anatase TiO<sub>2</sub> nanoparticles and study of optical properties and structural characterization of TiO<sub>2</sub>/MWCNT nanocomposite. *Optik* **2017**, *149*, 447–454. [[CrossRef](#)]
41. Kader, S.; Al-Mamun, M.R.; Suhan, M.B.K.; Shuchi, S.B.; Islam, M.S. Enhanced photodegradation of methyl orange dye under UV irradiation using MoO<sub>3</sub> and Ag doped TiO<sub>2</sub> photocatalysts. *Environ. Technol. Innov.* **2022**, *27*, 102476. [[CrossRef](#)]
42. Rahimnejad, S.; Setayesh, S.R.; Gholami, M.R. A credible role of copper oxide on structure of nanocrystalline mesoporous titanium dioxide. *J. Iran. Chem. Soc.* **2008**, *5*, 367–374. [[CrossRef](#)]
43. Yuan, Y.J.; Shen, Z.; Wu, S.; Su, Y.; Pei, L.; Ji, Z.; Ding, M.; Bai, W.; Chen, Y.; Yu, Z.T.; et al. Liquid exfoliation of g-C<sub>3</sub>N<sub>4</sub> nanosheets to construct 2D-2D MoS<sub>2</sub>/g-C<sub>3</sub>N<sub>4</sub> photocatalyst for enhanced photocatalytic H<sub>2</sub> production activity. *Appl. Catal. B Environ.* **2019**, *246*, 120–128. [[CrossRef](#)]
44. Talami, B.; Zeghioud, H.; Dalhatou, S.; Bonnet, P.; Caperaa, C.; Ligny, R.; Assadi, A.A.; Massai, H.; Kane, A. A new sunlight active photocatalyst based on CuO-TiO<sub>2</sub>-Clay composite for wastewater remediation: Mechanistic insights and degradation optimization. *Water Air Soil Pollut.* **2024**, *235*, 104. [[CrossRef](#)]
45. Perarasan, T.; Peter, I.J.; Kumar, A.M.; Rajamanickam, N.; Ramachandran, K.; Mohan, C.R. Copper doped titanium dioxide for enhancing the photovoltaic behavior in solar cell. *Mater. Today Proc.* **2019**, *35*, 66–68. [[CrossRef](#)]
46. Yoong, L.S.; Chong, F.K.; Dutta, B.K. Development of copper-doped TiO<sub>2</sub> photocatalyst for hydrogen production under visible light. *Energy* **2009**, *34*, 1652–1661. [[CrossRef](#)]
47. Liang, J.; Wang, J.; Yu, K.; Song, K.; Wang, X.; Liu, W.; Hou, J.; Liang, C. Enhanced photocatalytic performance of Nd<sup>3+</sup>-doped TiO<sub>2</sub> nanosphere under visible light. *Chem. Phys.* **2020**, *528*, 110538. [[CrossRef](#)]
48. Ma, H.; Zheng, W.; Yan, X.; Li, S.; Zhang, K.; Liu, G.; Jiang, L. Polydopamine-induced fabrication of Ag-TiO<sub>2</sub> hollow nanospheres and their application in visible-light photocatalysis. *Colloids Surf. A Physicochem. Eng. Asp.* **2020**, *586*, 2–7. [[CrossRef](#)]
49. Kerour, A.; Boudjadar, S.; Bourzami, R.; Allouche, B. Eco-friendly synthesis of cuprous oxide (Cu<sub>2</sub>O) nanoparticles and improvement of their solar photocatalytic activities. *J. Solid State Chem.* **2018**, *263*, 79–83. [[CrossRef](#)]
50. Javanroudi, S.R.; Fattahi, N.; Sharafi, K.; Arfaeina, H.; Moradi, M. Chalcopyrite as an oxidants activator for organic pollutant remediation: A review of mechanisms, parameters, and future perspectives. *Heliyon* **2023**, *9*, e19992. [[CrossRef](#)]
51. Kiwaan, H.A.; Atwee, T.M.; Azab, E.A.; El-Bindary, A.A. Photocatalytic degradation of organic dyes in the presence of nanostructured titanium dioxide. *J. Mol. Struct.* **2020**, *1200*, 127115. [[CrossRef](#)]

52. Isai, K.A.; Shrivastava, V.S. Photocatalytic degradation of methylene blue using ZnO and 2%Fe–ZnO semiconductor nanomaterials synthesized by sol–gel method: A comparative study. *SN Appl. Sci.* **2019**, *1*, 1247. [CrossRef]
53. Baaloudj, O.; Nasrallah, N.; Kebir, M.; Khezami, L.; Amrane, A.; Assadi, A.A. A comparative study of ceramic nanoparticles synthesized for antibiotic removal: Catalysis characterization and photocatalytic performance modeling. *Environ. Sci. Pollut. Res.* **2021**, *28*, 13900–13912. [CrossRef]
54. Aissani, T.; Yahiaoui, L.; Boudrahem, F.; Cherif, L.Y.; Fourcad, F.; Amrane, A.; Aissani-Benissad, F. Sulfamethazine degradation by heterogeneous photocatalysis with ZnO immobilized on a glass plate using the heat attachment method and its impact on the biodegradability. *React. Kinet. Mech. Catal.* **2020**, *131*, 471–487. [CrossRef]
55. Zeghioud, H.; Khellaf, N.; Amrane, A.; Djelal, H.; Elfalleh, W.; Assadi, A.A.; Rtimi, S. Photocatalytic performance of TiO<sub>2</sub> impregnated polyester for the degradation of Reactive Green 12: Implications of the surface pretreatment and the microstructure. *J. Photochem. Photobiol. A Chem.* **2017**, *346*, 493–501. [CrossRef]
56. Mouhamadou, S.; Dalhatou, S.; Obada, D.O.; Fryda, L.; Mahieu, A.; Bonnet, P.; Caperaa, C.; Kane, A.; Massai, H.; Zeghioud, H. Synthesis of piliostigma reticulatum decorated TiO<sub>2</sub> based composite and its application towards Cr(VI) adsorption and bromophenol blue degradation: Nonlinear kinetics, equilibrium modelling and optimisation photocatalytic parameters. *J. Environ. Chem. Eng.* **2023**, *11*, 109273. [CrossRef]
57. Almansba, A.; Kane, A.; Nasrallah, N.; Maachi, R.; Lamaa, L.; Peruchon, L.; Brochier, C.; Béchohra, I.; Amrane, A.; Assadi, A.A. Innovative photocatalytic luminous textiles optimized towards water treatment: Performance evaluation of photoreactors. *Chem. Eng. J.* **2021**, *416*, 129195. [CrossRef]
58. Kumar, K.V.; Porkodi, K.; Rocha, F. Langmuir–Hinshelwood kinetics—A theoretical study. *Catal. Commun.* **2008**, *9*, 82–84. [CrossRef]
59. Almansba, A.; Kane, A.; Nasrallah, N.; Wilson, J.M.; Maachi, R.; Lamaa, L.; Peruchon, L.; Brochier, C.; Amrane, A.; Assadi, A.A. An engineering approach towards the design of an innovative compact photo-reactor for antibiotic removal in the frame of laboratory and pilot-plant scale. *J. Photochem. Photobiol. A Chem.* **2021**, *418*, 113445. [CrossRef]
60. Nasr, O.; Mohamed, O.; Al-Shirbini, A.S.; Abdel-Wahab, A.M. Photocatalytic degradation of acetaminophen over Ag, Au and Pt loaded TiO<sub>2</sub> using solar light. *J. Photochem. Photobiol. A Chem.* **2019**, *374*, 185–193. [CrossRef]
61. Tamaddon, F.; Nasiri, A.; Yazdanpanah, G. Photocatalytic degradation of ciprofloxacin using CuFe<sub>2</sub>O<sub>4</sub>@methyl cellulose based magnetic nanobiocomposite. *MethodsX* **2020**, *7*, 74–81. [CrossRef]
62. Singh, P.; Vishnu, M.C.; Sharma, K.K.; Borthakur, A.; Srivastava, P.; Pal, D.B.; Tiwary, D.; Mishra, P.K. Photocatalytic degradation of Acid Red dye stuff in the presence of activated carbon-TiO<sub>2</sub> composite and its kinetic enumeration. *J. Water Process Eng.* **2016**, *12*, 20–31. [CrossRef]
63. Chekir, N.; Tassalit, D.; Benhabiles, O.; Merzouk, N.K.; Ghenna, M.; Abdessemed, A.; Issaadi, R. A comparative study of tartrazine degradation using UV and solar fixed bed reactors. *Int. J. Hydrogen Energy* **2017**, *42*, 8948–8954. [CrossRef]
64. Zyoud, A.H.; Zubi, A.; Hejjawi, S.; Zyoud, S.H.; Helal, M.H.; Zyoud, S.H.; Qamhieh, N.; Hajamohideen, A.R.; Hilal, H.S. Removal of acetaminophen from water by simulated solar light photodegradation with ZnO and TiO<sub>2</sub> nanoparticles: Catalytic efficiency assessment for future prospects. *J. Environ. Chem. Eng.* **2020**, *8*, 104038. [CrossRef]
65. Surya, L.; Sheilatin; Praja, P.V.; Sepia, N.S. Preparation and characterization of titania/bentonite composite application on the degradation of naphthol blue black dye. *Res. J. Chem. Environ.* **2018**, *22*, 48–53.
66. Essandoh, M.; Garcia, R.A. Efficient removal of dyes from aqueous solutions using a novel hemoglobin/iron oxide composite. *Chemosphere* **2018**, *206*, 502–512. [CrossRef]
67. Ahmed, A.; Abouseoud, M.; Couvert, A.; Amrane, A. Enzymatic degradation of Congo Red by turnip (*Brassica rapa*) peroxidase. *Z. Naturforsch. Sect. C J. Biosci.* **2012**, *67*, 429–436. [CrossRef]
68. Christy, E.J.S.; Amalraj, A.; Rajeswari, A.; Pius, A. Enhanced photocatalytic performance of Zr(IV) doped ZnO nanocomposite for the degradation efficiency of different azo dyes. *Environ. Chem. Ecotoxicol.* **2021**, *3*, 31–41. [CrossRef]
69. Dhatsanamurthi, P.; Shanthi, M. Enhanced photocatalytic degradation of azo dye in aqueous solutions using Ba@Ag@ZnO nanocomposite for self-sensitized under sunshine irradiation. *Int. J. Hydrogen Energy* **2017**, *42*, 5523–5536. [CrossRef]
70. Rauf, M.A.; Meetani, M.A.; Hisaindee, S. An overview on the photocatalytic degradation of azo dyes in the presence of TiO<sub>2</sub> doped with selective transition metals. *Desalination* **2011**, *276*, 13–27. [CrossRef]
71. Karthikeyan, P.; Elanchezhian, S.S.D.; Ali, H.; Banu, T.; Farzana, M.H.; Min, C. Chemosphere Hydrothermal synthesis of hydroxyapatite-reduced graphene oxide (1D e 2D) hybrids with enhanced selective adsorption properties for methyl orange and hexavalent chromium from aqueous solutions. *Chemosphere* **2021**, *276*, 130200. [CrossRef]
72. Hassan, F.; Bonnet, P.; Marie, J.; Dikdim, D.; Bandjoun, N.G.; Caperaa, C.; Dalhatou, S.; Kane, A.; Zeghioud, H. Synthesis and Investigation of TiO<sub>2</sub>/g-C<sub>3</sub>N<sub>4</sub> Performance for Photocatalytic Degradation of Bromophenol Blue and Eriochrome Black T: Experimental Design Optimization and Reactive Oxygen Species Contribution. *Water* **2022**, *14*, 3331. [CrossRef]
73. Shahnaz, T.; Sharma, V.; Subbiah, S.; Narayanasamy, S. Multivariate optimisation of Cr (VI), Co (III) and Cu (II) adsorption onto nanobentonite incorporated nanocellulose/chitosan aerogel using response surface methodology. *J. Water Process Eng.* **2020**, *36*, 101283. [CrossRef]
74. Zhang, J.; Fu, D.; Xu, Y.; Liu, C. Optimization of parameters on photocatalytic degradation of chloramphenicol using TiO<sub>2</sub> as photocatalyst by response surface methodology. *J. Environ. Sci.* **2010**, *22*, 1281–1289. [CrossRef] [PubMed]

75. Çatlıoğlu, F.; Akay, S.; Turunç, E.; Gözmen, B.; Anastopoulos, I.; Kayan, B.; Kalderis, D. Preparation and application of Fe-modified banana peel in the adsorption of methylene blue: Process optimization using response surface methodology. *Environ. Nanotechnol. Monit. Manag.* **2021**, *16*, 100517. [[CrossRef](#)]
76. Sohrabi, S.; Akhlaghian, F. Modeling and optimization of phenol degradation over copper-doped titanium dioxide photocatalyst using response surface methodology. *Process Saf. Environ. Prot.* **2016**, *99*, 120–128. [[CrossRef](#)]
77. Evgenidou, E.; Chatzisalata, Z.; Tsevis, A.; Bourikas, K.; Torounidou, P.; Sergelidis, D.; Koltsakidou, A.; Lambropoulou, D.A. Photocatalytic degradation of a mixture of eight antibiotics using Cu-modified TiO<sub>2</sub> photocatalysts: Kinetics, mineralization, antimicrobial activity elimination and disinfection. *J. Environ. Chem. Eng.* **2021**, *9*, 105295. [[CrossRef](#)]
78. Malesic-Eleftheriadou, N.; Evgenidou, E.; Kyzas, G.Z.; Bikiaris, D.N.; Lambropoulou, D.A. Removal of antibiotics in aqueous media by using new synthesized bio-based poly(ethylene terephthalate)-TiO<sub>2</sub> photocatalysts. *Chemosphere* **2019**, *234*, 746–755. [[CrossRef](#)]

**Disclaimer/Publisher's Note:** The statements, opinions and data contained in all publications are solely those of the individual author(s) and contributor(s) and not of MDPI and/or the editor(s). MDPI and/or the editor(s) disclaim responsibility for any injury to people or property resulting from any ideas, methods, instructions or products referred to in the content.